NEUROPHYSIOLOGY

The long noncoding RNA *neuroLNC* regulates presynaptic activity by interacting with the neurodegeneration-associated protein TDP-43

S. Keihani[1]*, V. Kluever[1]*, S. Mandad[1,2], V. Bansal[3,4], R. Rahman[3], E. Fritsch[1], L. Caldi Gomes[5,6], A. Gärtner[7], S. Kügler[5], H. Urlaub[2,8], J. D. Wren[9], S. Bonn[3,4], S. O. Rizzoli[1,6], E. F. Fornasiero[1,6†]

The cellular and the molecular mechanisms by which long noncoding RNAs (lncRNAs) may regulate presynaptic function and neuronal activity are largely unexplored. Here, we established an integrated screening strategy to discover lncRNAs implicated in neurotransmitter and synaptic vesicle release. With this approach, we identified *neuroLNC*, a neuron-specific nuclear lncRNA conserved from rodents to humans. *NeuroLNC* is tuned by synaptic activity and influences several other essential aspects of neuronal development including calcium influx, neuritogenesis, and neuronal migration in vivo. We defined the molecular interactors of *neuroLNC* in detail using chromatin isolation by RNA purification, RNA interactome analysis, and protein mass spectrometry. We found that the effects of *neuroLNC* on synaptic vesicle release require interaction with the RNA-binding protein TDP-43 (TAR DNA binding protein-43) and the selective stabilization of mRNAs encoding for presynaptic proteins. These results provide the first proof of an lncRNA that orchestrates neuronal excitability by influencing presynaptic function.

INTRODUCTION

Long noncoding RNAs (lncRNAs) are defined as RNA transcripts longer than 200 nucleotides that show no evidence of protein coding potential (*1*). While initially considered a "noisy" by-product of pervasive eukaryotic genome transcription (*2*), novel roles of lncRNAs have begun to emerge, and their investigation is rapidly gaining momentum in multiple fields of biology (*3*). Their significance is especially salient in the field of cancer biology, where lncRNAs have been found to be excellent biomarkers for predicting phenotypic changes in malignancies (*4*).

In the brain, the high abundance and strict developmental regulation of lncRNAs suggest that these molecules have bona fide regulatory functions in neuronal differentiation and possibly play a role in the establishment of disease (*5*, *6*). Since lncRNAs can be rapidly turned over (*7*), their function might be of particular importance to the swift fine-tuning of synaptic activity during the delicate establishment of neuronal circuits and during continuous structural plasticity in the brain (*8–10*). Thus, it is imperative to understand the precise biological roles of these molecules in brain development and neuronal activation.

Notwithstanding, the importance of lncRNAs in the brain is often underestimated because of the inherent difficulty in designing coherent experimental strategies. A major confounding factor in these studies is the nonstringent transcription of neighboring genes, which often leads to false-positive correlations for lncRNAs that do not have a "true" molecular function. As a result, the number of candidates that need to be screened in these experiments is disproportionately high, and they provide relatively few functional lncRNAs. Moreover, the heterogeneous nature of the lncRNAs' molecular functions means that their discovery necessitates the use of highly complex and often unestablished analysis techniques (*11*). These factors have inarguably hindered the study of lncRNAs, despite the biological significance of these molecules.

To gain more insight into the role of lncRNAs in the regulation of neuronal activity, here, we have developed a two-step screening strategy that lessens the confounding effect of pervasive transcription. Our approach takes advantage of a bioinformatic preselection, which screens for conserved correlation across species, followed by an assay for measuring synaptic vesicle (SV) exo-endocytosis, where the lncRNAs of interest are overexpressed. Because of the initial overexpression, we were able to discard all candidates that do not have a "true" molecular function early on in our experimental workflow. Our approach has allowed us to identify an lncRNA that we named *neuroLNC*, which is highly neurospecific and developmentally regulated and controls several crucial aspects of neuronal physiology. We also examined the molecular interactions of *neuroLNC* in detail with omics strategies and found that it interacts with the RNA-binding protein TDP-43 (TAR DNA binding protein-43) and promotes the selective stabilization of mRNAs encoding for presynaptic proteins. We propose that *neuroLNC* orchestrates neuronal excitability and influences the posttranscriptional regulation of a set of transcripts by serving as a nuclear organizing hub, implicating TDP-43 in the coordination of neurotransmitter release. More extensively, *neuroLNC* may be essential for ensuring efficient structural plasticity, and due to its interaction with TDP-43, might play a role in the modulation of disease states.

[1]Department of Neuro- and Sensory Physiology, University Medical Center Göttingen, Excellence Cluster Multiscale Bioimaging, 37073 Göttingen, Germany. [2]Department of Clinical Chemistry, University Medical Center Göttingen, 37077 Göttingen, Germany. [3]Institute of Medical Systems Biology, Center for Molecular Neurobiology (ZMNH), UKE, 20246 Hamburg, Germany. [4]German Center for Neurodegenerative Diseases (DZNE), 72076 Tübingen, Germany. [5]Department of Neurology, University Medical Center Göttingen, 37073 Göttingen, Germany. [6]Center for Biostructural Imaging of Neurodegeneration (BIN), 37075 Göttingen, Germany. [7]VIB Center for the Biology of Disease and Center for Human Genetics, KU Leuven, Leuven, Belgium. [8]Bioanalytical Mass Spectrometry Group, Max Planck Institute of Biophysical Chemistry, 37077 Göttingen, Germany. [9]Department of Genes and Human Disease, Oklahoma Medical Research Foundation, Oklahoma City, OK 73104, USA.
*These authors contributed equally to this work as first authors.
†Corresponding author. Email: efornas@gwdg.de

RESULTS

A screening strategy for lncRNAs involved in SV release identifies *neuroLNC* as a critical regulator of neurotransmitter release

While the roles of lncRNAs during neurogenesis and in the early steps of neuronal development have been more intensively studied (*12*), their importance during terminal differentiation, and in particular, in SV exo-endocytosis, is virtually unknown. We thus decided to specifically study this process, which arises relatively late during neuronal differentiation (*13*). To this aim, we developed a two-step screening strategy for identifying lncRNAs that regulate neurotransmitter release in primary neurons. Our strategy combines an initial "guilt by association" bioinformatic approach [global microarray meta-analysis (GAMMA)] based on correlation networks constructed using public transcriptional data (*14*) and a subsequent assay for measuring SV release based on a genetically encoded reporter (Fig. 1A) (*15*). When applying this approach, our GAMMA query yielded a total of 79 lncRNA candidates. We filtered these further to include only those transcripts that are distant from protein-coding genes conserved in rats, mice, and humans (data S1A). The resulting six candidates, detailed in data S1B, were cloned and further tested in an SV release assay. This allowed us to identify an lncRNA, "uc003wst.1," which upon overexpression drastically increases the release of SVs in primary rat hippocampal neurons [351 and 268% increases following 60 and 600 action potentials (APs), respectively; Fig. 1, B and C, and fig. S1A], without affecting the total vesicle pool size (fig. S1B). This lncRNA only partially overlaps with the previously annotated *LINC00599*, depending on the gene assembly and the species analyzed (data S1B). Hence, to avoid confusion, we named it "*neuroLNC*." Down-regulation of endogenous *neuroLNC* by short hairpin RNAs (shRNAs) resulted in decreased SV release (Fig. 1, D and E, and fig. S1, C to G), showing that its expression levels are directly related to the extent of neurotransmission.

NeuroLNC is conserved in rodents and humans, and its genomic locus is close to *miR-124-1*

Since lncRNAs can exert their function by influencing the transcripts in cis in their close proximity, we characterized the *neuroLNC* locus and its genomic organization in detail. *NeuroLNC* is highly conserved between rat and mouse, showing an overall 90.4% similarity and 87.7% identity. Orthologous analysis in rat, mouse, and human shows that for all three organisms its sequences have very low coding potential (fig. S2A) and that they share two conserved regions (CR1 and CR2) with ~80% homology, in agreement with what is observed for other notable lncRNAs (fig. S2B) (*16*). The genomic localization and the expression of *neuroLNC* are conserved among rodents and humans. While the gene itself is located on different chromosomes for different species, it always shares synteny with *miR-124-1*, the most abundant microRNA (miRNA) expressed in neurons (Fig. 1F and fig. S2, C to E) (*17*). Proximity to an miRNA is expected since regions harboring lncRNAs can be organized in complex polycistronic clusters together with several miRNAs (*18*). Yet, despite the fact that there is a correlation between *neuroLNC* and *miR-124-1* expression (Fig. 2A), we established that *neuroLNC* is a separate entity from this miRNA (Fig. 2, B and C). For this, we isolated total RNA and genomic DNA [as a polymerase chain reaction (PCR) control] from rat. The RNA was retrotranscribed with random priming and PCR-amplified to reveal the presence of different RNA species. If upon retrotranscription the PCR was positive for a specific couple of primers, then it indicated

that there are RNA molecules spanning the region. On the contrary, the absence of amplification suggested that there are no RNAs spanning the entire region. In total, eight different couples of primers were designed for the region between *miR-124-1* and *neuroLNC*, and 13 different amplification reactions were tested. While the presence of several isoforms of *neuroLNC* is likely, there is, however, no continuity between *miR-124-1* and *neuroLNC*. Moreover, *neuroLNC* does not interfere in cis with either *miR-124-1* expression levels or its processing, measured by comparing relative levels of its 3p and 5p forms using miRNA specific quantitative polymerase chain reaction (miQPCR) (Fig. 2, D to F) (*19*). For the sake of completeness, we also characterized the distribution of the transcriptional starting sites (TSS) in the *miR-124-1/neuroLNC* locus. The region harbors at least 30 TSS, which give rise to several transcripts in both sense and antisense directions with respect to both *miR-124-1* and *neuroLNC*, confirming our PCR results (Fig. 2G and data S1C). This observation is also in line with what has been previously observed, since several lncRNAs exhibit multiple splicing isoforms and TSS, which may contribute to cell type–specific or developmental stage–specific events (*20*). Although this complex picture suggests the presence of several *neuroLNC* isoforms, here, we focused on the original *neuroLNC* as was defined in our bioinformatic screening (detailed in data S1B).

NeuroLNC is highly neurospecific, developmentally regulated, and activity dependent and influences calcium dynamics

We found that *neuroLNC* expression is highly restricted to the brain (Figs. 2A and 3A) and more specifically to the nucleus of neuronal cells (Fig. 3, B and C, and fig. S3A), while it is virtually undetectable in glial cells and cell lines used for modeling neuronal cells (fig. S3B). *NeuroLNC* is developmentally regulated in vitro since its levels initially peak during early development and then even out with aging (fig. S3C). In the rat brain in vivo, its expression is highest at P7 and is reduced to ~30% of its maximum in adults (fig. S3D). *NeuroLNC* expression in adults can still be detected in human brains as well (fig. S3E), suggesting a function that goes beyond differentiation and is kept during the entire life span of neurons.

Having confirmed the neurospecificity of *neuroLNC* and its involvement in terminal neuronal differentiation, we tested whether it could also affect presynaptic Ca²⁺ dynamics. Primary rat hippocampal neurons infected with an adeno-associated virus (AAV) overexpressing *neuroLNC* showed a significantly enhanced Ca²⁺ influx following a stimulation of 20 AP at 5 and 10 Hz but not at 80 Hz (Fig. 3D and fig. S4, A to C). On the contrary, *neuroLNC* down-regulation decreases the influx of Ca²⁺ during a prolonged 600-AP stimulation at 20 Hz (Fig. 3E). *NeuroLNC* levels also affect the frequencies of endogenous calcium bursts that can be observed in hippocampal cultures (Fig. 3F and fig. S4D) (*21*). Having demonstrated that *neuroLNC* is linked to neuronal activity, we turned to investigating whether the regulation of neuronal activity can influence the endogenous expression of *neuroLNC*. We tested this in terminally differentiated neurons [>14 days in vitro (DIV)], using single-molecule fluorescence in situ hybridization (FISH), and we evaluated whether a modulation of neuronal activity has an effect on the number of *neuroLNC* foci. While blocking neuronal activity with either tetrodotoxin (TTX) or 6-cyano-7-nitro-quinoxaline-2,3-dione (CNQX) had no direct effect on *neuroLNC* foci numbers, pharmacological intensification of neuronal activity with bicuculline or 4-aminopyridine (4-AP) significantly increased the number of foci 5 hours after treatment (Fig. 3G).
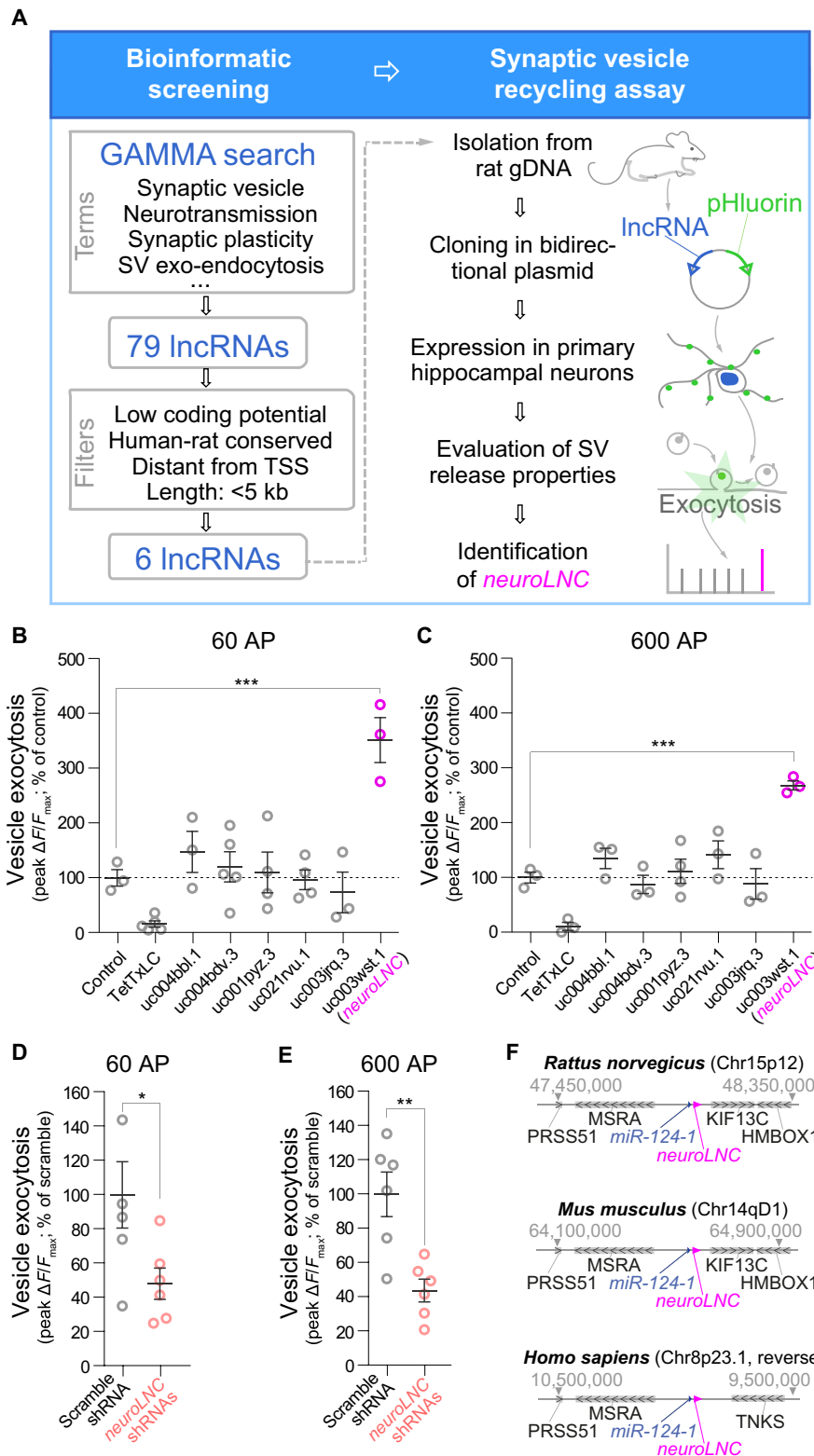
Fig. 1. An integrated screening strategy identifies *NeuroLNC*, a conserved lncRNA that regulates SV release. (**A**) Scheme depicting the experimental steps of the bio-informatic strategy and of the SV assay. gDNA, genomic DNA. (**B**) Quantification of the pHluorin experiments upon the pBI-driven overexpression of the lncRNAs following 60-AP field stimulation at 20 Hz. Mean values are plotted (± SEM). The tetanus toxin light chain (TetTxLC) was used as a negative control. Statistical test, one-way analysis of variance (ANOVA) followed by Bonferroni's multiple comparison test versus control (***$P < 0.001$). (**C**) Quantification and statistics as in (B), following a 600-AP field stimulation at 20 Hz. (**D** and **E**) Quantification of the SV exo-endocytosis experiments following either a 60- or 600-AP 20-Hz field stimulation, respectively, upon *neuroLNC* down-regulation. Statistical test, unpaired two-tailed Student's *t* test (*$P < 0.05$ and **$P < 0.01$). (**F**) Schematic representation of the genomic locus of *neuroLNC* for rat, mouse, and human.
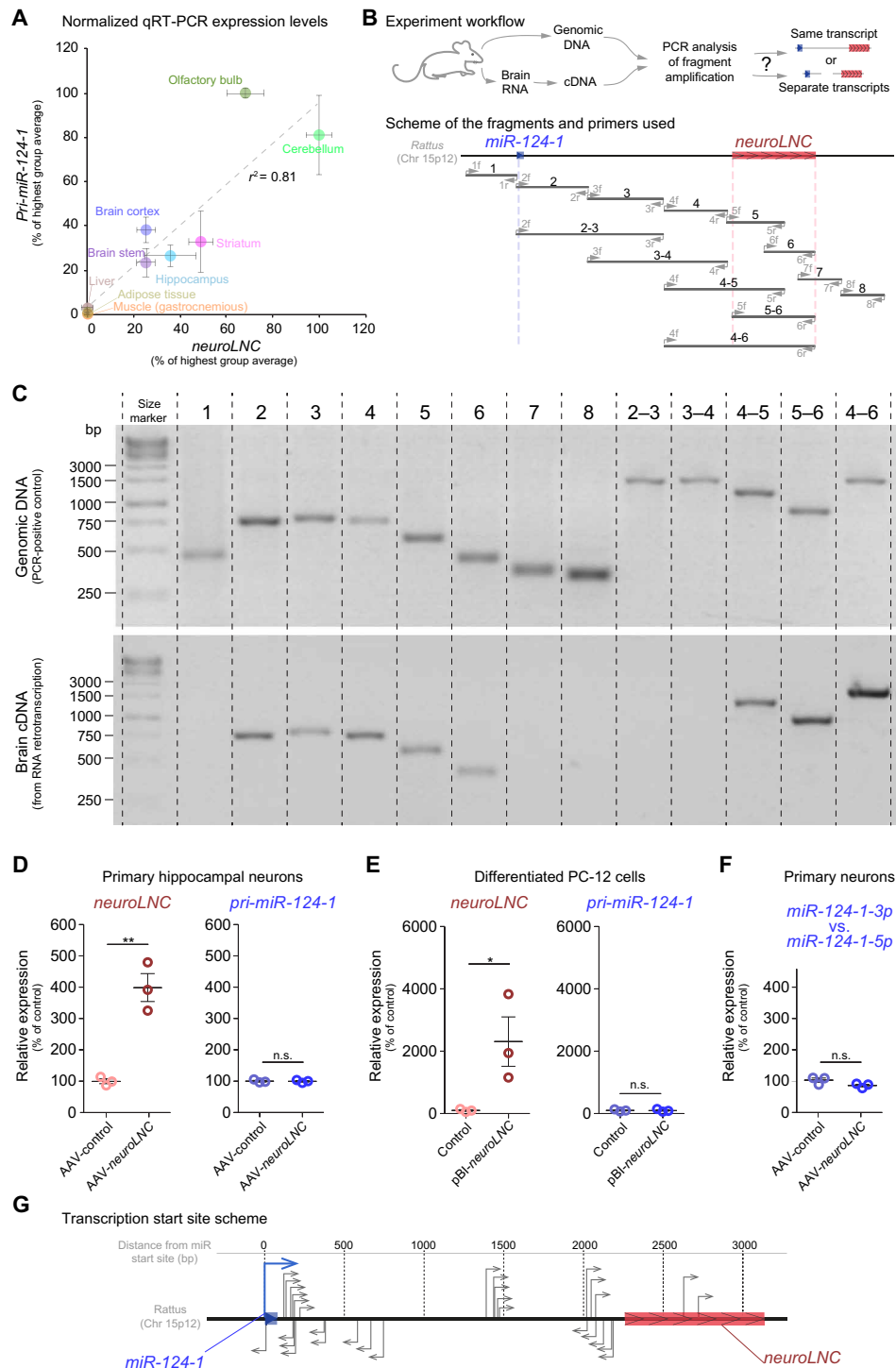
Fig. 2. *NeuroLNC* and miRNA 124-1 are two separate entities with distinct TSS. (**A**) Scatter plot showing the expression of *neuroLNC* and *pri-miR-124-1*. Since the two RNAs are transcribed from nearby genomic regions, we tested the correlation of the expression of the two RNAs ($r^2 = 0.81$). (**B**) Experimental strategy used to test the presence of different RNA transcripts in the region between *pri-miR-124-1* and *neuroLNC*. In the lower panel, the couple of primers used (light gray) and the fragments amplified (black) are represented to scale. (**C**) Results of the experiment exemplified in (B). The upper panel corresponds to the control PCR reaction on genomic DNA, and the lower panel shows the amplification of the retrotranscribed brain RNA. The lack of continuity between *neuroLNC* and *mirR-124-1* (regions 2 and 3 and regions 3 and 4) indicates separate entities. For details concerning the primer sequences, refer to data S1J. bp, base pair; cDNA, complementary DNA. (**D** and **E**) Overexpression of *neuroLNC* in either primary hippocampal neurons (D) or differentiated PC-12 cells (E) does not influence the expression of *pri-miR-124-1*. The expression level values plotted are expressed as a percentage of the AAV-control or the control plasmid. *NeuroLNC* is significantly overexpressed, but there is no effect on the levels of *pri-miR-124-1*. Statistical tests, two-tailed Student's *t* test (*$P < 0.05$ and **$P < 0.01$); n.s., not significant. (**F**) *NeuroLNC* overexpression does not influence the processing of *miR-124-1* and the relative levels of its 3p and 5p forms. (**G**) TSS analysis. The scheme summarizes the observed starting sites, detailed in data S1C.
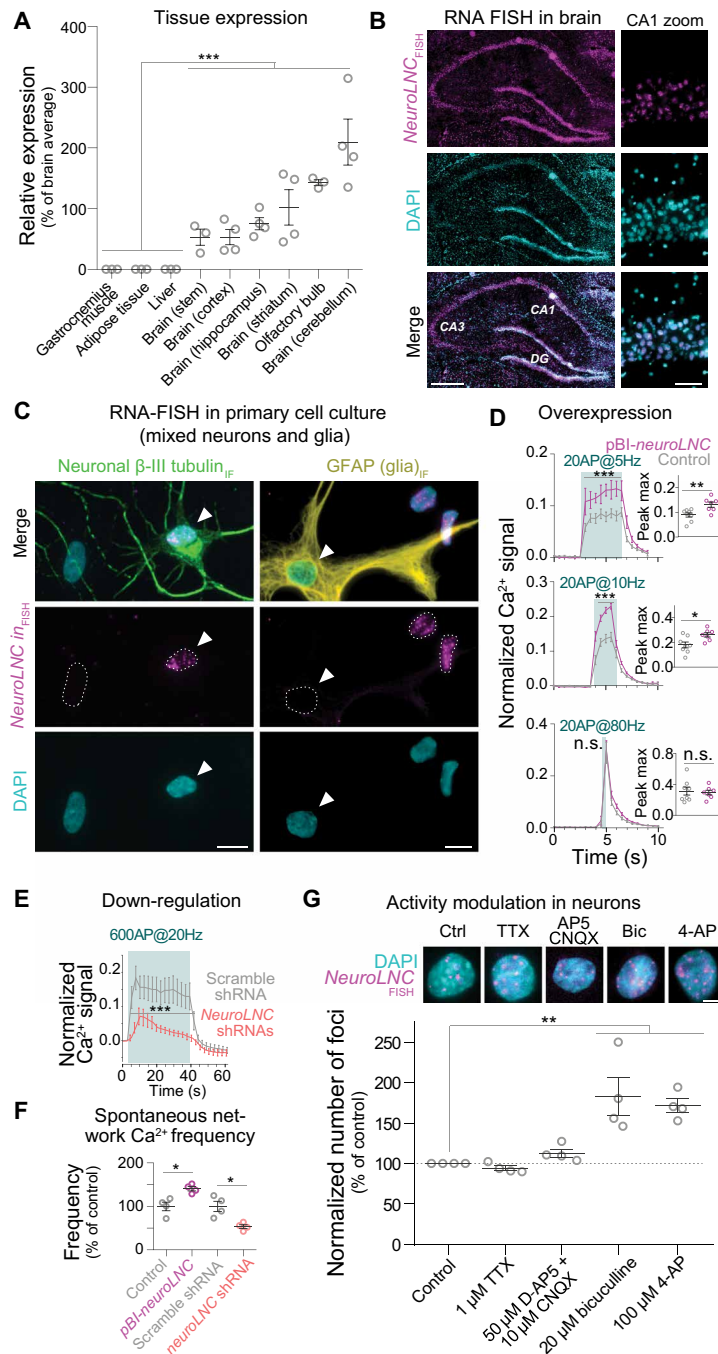
Fig. 3. *NeuroLNC* is neuron specific and nuclear, regulates presynaptic Ca^{2+} influx, and is modulated by neuronal activity. (**A**) Relative expression of *neuroLNC* in the rat central nervous system (CNS) and other tissues, as measured by quantitative real-time PCR (qRT-PCR). Statistical test, one-way ANOVA followed by Bonferroni's multiple comparison test versus all non-CNS samples (***$P < 0.001$). (**B**) RNA fluorescence in situ hybridization (RNA-FISH) of *neuroLNC* on coronal brain slice of rat (P14). Note the localization to the nuclei of *CA1* neurons in the zoom. Scale bars, 0.5 mm (left); 50 µm (right). DAPI, 4',6-diamidino-2-phenylindole. (**C**) Combined RNA-FISH and immunofluorescence in primary mixed neuroglial cultures. Note that β-III tubulin–positive neurons are *neuroLNC* positive (left, white arrowhead), while cells positive for the glial marker glial fibrillary acidic protein (GFAP) are *neuroLNC* negative (right, white arrowhead). Scale bars, 10 µm. (**D**) Quantification of Ca^{2+} influx in primary hippocampal neurons upon *neuroLNC* overexpression following a 20-AP field stimulation at different frequencies. Mean values are plotted (± SEM). Insets indicate the difference in fluorescence measured at the maximum peak for each experiment. Statistical test, unpaired two-tailed Student's *t* test (*$P < 0.05$; **$P < 0.01$; and ***$P < 0.001$). See fig. S5 for details. (**E**) Quantification of Ca^{2+} influx as in (D), following shRNA-mediated *neuroLNC* down-regulation with a 600-AP stimulation at 20 Hz. Upon *neuroLNC* down-regulation, Ca^{2+} influx is significantly decreased. (**F**) Physiological (unstimulated) network activity measured in neurons following overexpression or down-regulation of *neuroLNC*. Overexpression increases spontaneous activity, while down-regulation has the opposite effect. Unpaired two-tailed Student's *t* test (*$P < 0.05$). (**G**) The number of *neuroLNC* foci following activity modulation of neurons. Blocking the activity of neurons with TTX or AP5 + CNQX has no effect. The number of *neuroLNC* foci is promoted by increasing neuronal activity by applying bicuculline or 4-AP. In the upper panels, representative images are shown. Scale bar, 5 µm. Normalized averages are shown. One-way ANOVA followed by Bonferroni's multiple comparison test versus control (**$P < 0.01$).

NeuroLNC regulates neurite elongation in vitro and neuronal migration in vivo

Given the role of lncRNAs and Ca^{2+} dynamics in neuronal development (*12*, *22*) and the maximal expression of *neuroLNC* in the young brain (fig. S3D), it appeared likely that *neuroLNC* could also influence other developmental aspects in neurons. We therefore studied the role of *neuroLNC* in neurite growth in an in vitro assay that is used as a paradigm to study early neuronal development. Down-regulation of *neuroLNC* in rat primary hippocampal neurons decreased both neurite length and branching (Fig. 4, A and B), while its overexpression had the opposite effect (Fig. 4, C and D). As neurite growth is instrumental for neuronal polarization and migration (*23*), we tested whether *neuroLNC* could also influence mouse cortical neuron migration in vivo. Following in utero electroporation of shRNA constructs under a pol III promoter (U6), the electroporated precursor cells in the ventricular zone (VZ) terminally differentiate and become neurons. Neurons move to reach their final position in the cortical plate (CP), migrating through the subventricular zone (SVZ) and intermediate zone (IZ), eventually establishing connections with the marginal zone (MZ). *NeuroLNC* down-regulation decreases the migration of neurons in vivo from the VZ to the CP (Fig. 4, E and F). *NeuroLNC* overexpression has the opposite effect, since neurons show a more efficient migration pattern from the SVZ with respect to the control (Fig. 4, G and H). Together, the results presented so far suggest that *neuroLNC* exerts regulatory effects on the biology of neurons at different developmental stages and likely participates in the fine-tuning of neurotransmission.

NeuroLNC interacts with DNA regions related to SV release and synapse organization

In neurons, lncRNAs may act as scaffolding adaptors in macromolecular complexes that finely regulate the execution of gene expression programs at different steps of mRNA and protein biogenesis (*12*). This could explain how a single molecular species can influence in trans several unrelated mechanisms such as neuritogenesis, calcium signaling, and neurotransmitter release. To test this hypothesis, we performed a series of experiments aimed at defining the molecular interactors of *neuroLNC* in vivo at the DNA, RNA, and protein level (Fig. 5A). Since *neuroLNC* is strictly nuclear (Fig. 3C), we first applied chromatin isolation by RNA purification (ChIRP) (*24*) from the rat brain cortex to identify the genome regions where *neuroLNC* may perform its regulatory function(s).

After confirming the specificity and the reliability of the experimental approach (fig. S5A), we found that *neuroLNC* interacts with the DNA regions of 3327 genes (Fig. 5B and data S1D). *neuroLNC* preferentially interacts with intronic regions (82%) and regions in the close vicinity of genes (16%), with a preference for upstream regions (Fig. 5B). This localization may suggest a function of *neuroLNC* in the transcription and/or splicing of these genes. Gene ontology (GO) analysis of the target genes shows that *neuroLNC* is significantly enriched in regions related to glutamate receptor signaling, regulation of membrane potential, and synapse organization (Fig. 5C and data S1E). These results are in line with the biological phenotype that we observe via *neuroLNC* modulation in neurons.

NeuroLNC binds a subset of mRNAs coding for SV proteins

To define the RNA molecules interacting with *neuroLNC*, we also characterized the RNAs that were coprecipitating during ChIRP in an RNA interactome experiment (Fig. 5, D and E, and data S1F).

NeuroLNC mostly interacts with coding mRNAs (~78% of hits), although, the fraction of interacting ncRNAs is higher than expected from pure chance (twofold higher, χ^2 statistic, 43.5; $P < 0.0001$; Fig. 5D). Among the most abundant mRNAs interacting with *neuroLNC*, there are two solute carriers (Slc35a1 and Slc22a12), the delta-like canonical Notch ligand 3 (Dll3), and three crucial mRNAs of proteins involved in neurotransmitter release (SNAP25, Stx1b, and Rab3c; Fig. 5E). The Notch signaling pathways have also been previously shown to be a target of *LncND*, an lncRNA that is enriched in radial glial cells in the VZ of the developing human brain (*25*). The fact that the overlap between the DNA-ChIRP and the RNA interactome analysis is limited (only 34 mRNAs, including Rab3c and Dll3 as detailed in data S1G) might reflect the heterogeneity of the complexes in which *neuroLNC* is involved.

NeuroLNC interacts with TDP-43, and the block of this interaction abolishes the effects of *neuroLNC* on neurotransmitter release

To define the protein interactors of *neuroLNC*, we also performed protein mass spectrometry (MS) upon *neuroLNC* enrichment, as previously described (Fig. 5, F and G; fig. S5B; and data S1H) (*26*). The sole highly significant enriched interactor of *neuroLNC* is the RNA-binding protein TDP-43, a central player in the pathogenesis of neurodegenerative disorders (*27*) such as frontotemporal lobar degeneration (FTLD; also known as frontotemporal dementia) and amyotrophic lateral sclerosis (ALS). We also found another important enriched player in ALS, the RNA-binding protein found in sarcoma (FUS), just below significance levels (enriched approximately seven times, $P = 0.058$).

Because of the importance of TDP-43, we studied its functional interactions with *neuroLNC* in more detail. We performed RNA immunoprecipitation (RIP) from the rat cortex with an antibody against TDP-43, and we confirmed that the endogenous TDP-43 in the brain is bound to *neuroLNC* (Fig. 5H and fig. S5C). Since TDP-43, which is mainly nuclear, can be delocalized to the cytosol during pathological modifications, we tested whether the overexpression of *neuroLNC* can delocalize it from the nucleus, but that was not the case (fig. S5D). Last, we tested whether there is any functional interaction between *neuroLNC* and TDP-43 in the same SV assay used in our initial SV screening (Fig. 5, I and J). To this purpose, TDP-43 was over-expressed or down-regulated (fig. S5E) in combination with *neuroLNC* overexpression. Since TDP-43 is known to bind a consensus sequence with uridine-guanine (UG)–repeats (*28*), we also included a mutated *neuroLNC*, where the UG-repeats were substituted (*neuroLNC*^{MUT}; data S1I). Transient overexpression of either *neuroLNC* or TDP-43 in rat neurons increased SV release, as expected from our results, and in line with previous results obtained with neurospecific TDP-43 transgenic mice (*29*). The effect of *neuroLNC* was blocked by the down-regulation of TDP-43 or by the expression of *neuroLNC*^{MUT} (Fig. 5, I and J). This indicates that at least some of the functions of *neuroLNC* are facilitated by its interaction with TDP-43.

NeuroLNC acts by increasing the levels of mRNA coding for SV proteins

Which is the molecular mechanism that allows *neuroLNC* to modulate presynaptic activity? It could be speculated that *neuroLNC* contributes to two distinct regulatory events, one at the level of chromatin, which regulates gene expression, and one specifically related to RNA biogenesis, splicing, or stabilization, which requires the corecruitment
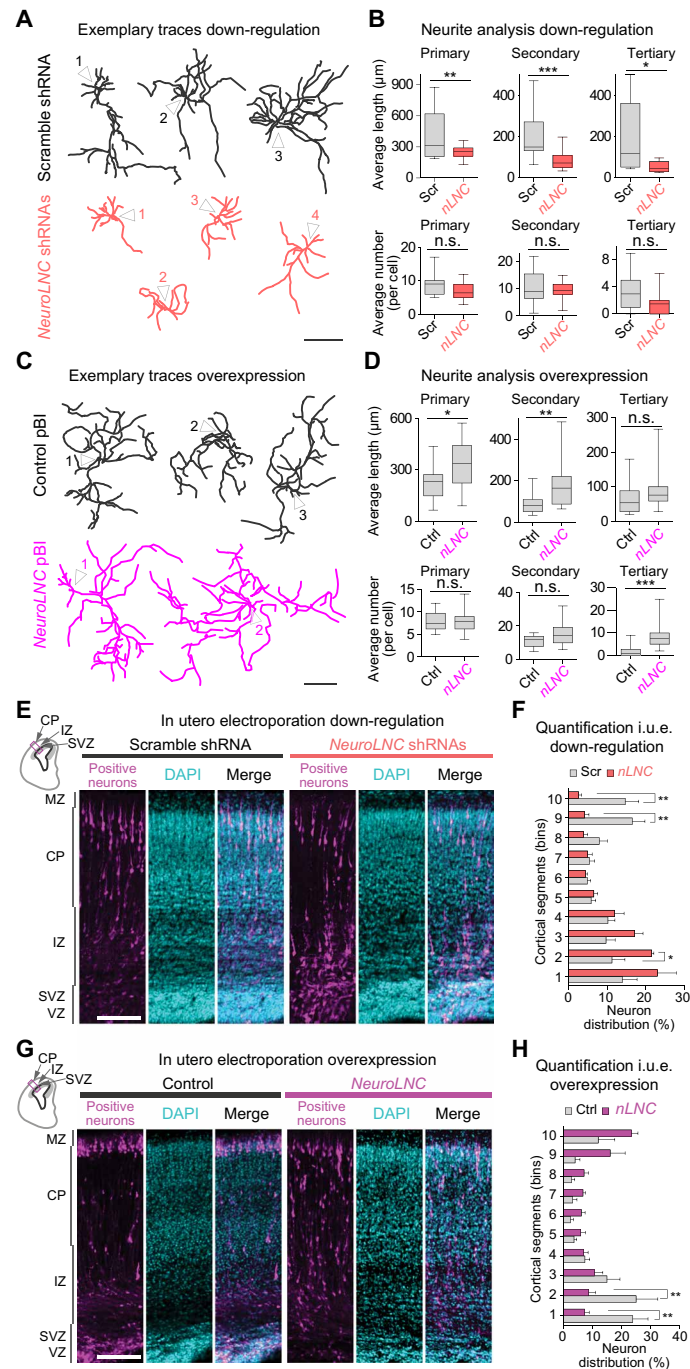
Fig. 4. *NeuroLNC* influences neurite elongation and branching in vitro and neuronal migration in vivo. (**A**) Exemplary traces of reconstructed primary hippocampal neurons transfected with either scramble shRNAs or a pool of three shRNAs against *neuroLNC*. White arrowheads indicate position of the cell body, and numbers designate different cells. Scale bar, 250 μm. (**B**) Summary of morphometric analysis on reconstructed neurons upon *neuroLNC* down-regulation. Box plots summarize the data distribution of ~700 neurites as explained in the methods. Unpaired two-tailed Student's *t* test (*$P < 0.05$; **$P < 0.01$; and ***$P < 0.001$). (**C**) Exemplary traces of reconstructed neurons as in (A), but upon *neuroLNC* overexpression. Scale bar, 250 μm. (**D**) Summary of the morphometric analysis of reconstructed neurons. Tracing and analysis of ~1000 neurites as in (B). (**E**) Exemplary confocal images of neuronal cells in E17.5 mouse cortices following E14.5 in utero electroporation (i.u.e.) with either scramble shRNAs or the shRNA pool against *neuroLNC*. Upper-left inset represents the portion of the coronal section imaged. Green fluorescent protein (GFP) was included for visualization of electroporated neurons (positive neurons are color-coded in magenta). Scale bar, 100 μm. (**F**) Frequency distribution and quantification of positive neurons upon *neuroLNC* down-regulation from the VZ (1st cortical segment) to the CP (10th cortical segment). Equal bins are used and data indicate mean ± SEM (experimental $n = 5$ in control and 7 in *neuroLNC* down-regulation). Two-way ANOVA with Bonferroni multiple comparison test for each single bin (*$P < 0.05$ and **$P < 0.01$). (**G**) Exemplary confocal images showing *neuroLNC* overexpression in an i.u.e. designed as in (E). A GFP version of the same plasmid was used as a negative control and coelectroporated for identifying positive neurons (color-coded in magenta). Scale bar, 100 μm. (**H**) Frequency distribution and quantification of positive neurons upon *neuroLNC* overexpression performed as in (F). Experimental $n = 6$ in both control *neuroLNC* overexpression. Two-way ANOVA with Bonferroni multiple comparison test for single bin pairs (**$P < 0.01$).
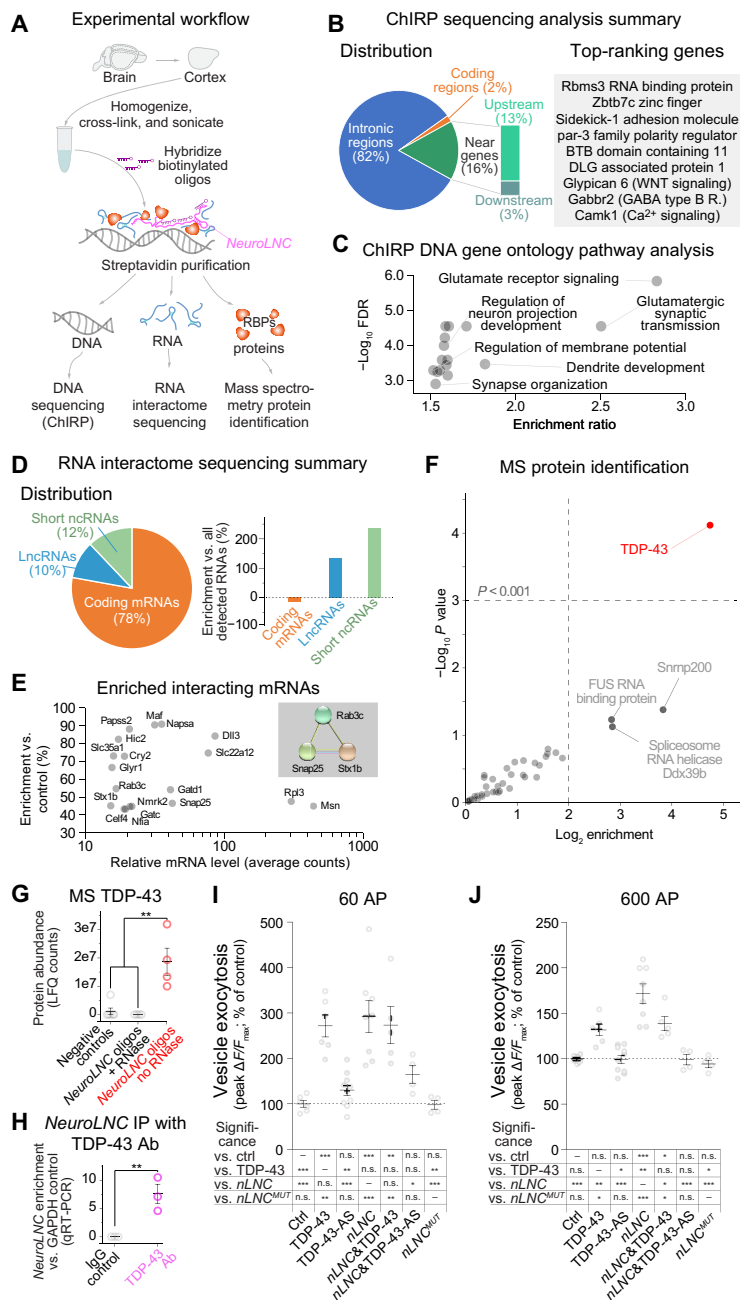
Fig. 5. *NeuroLNC* interacts in vivo with DNA and mRNA sequences of genes implicated in synaptic transmission, binds TDP-43, and requires its presence for modulating SV exocytosis. (**A**) Experimental workflow. For details and controls, see Materials and Methods and fig. S6. RBP, RNA binding protein. (**B**) Summary of DNA interactors of *neuroLNC*. All the hits are in data S1D. Among genes, preferentially bound top-ranking are shown in the gray inset. (**C**) Scatter plot of the false discovery rate (FDR, expressed as −log$_{10}$) and enrichment ratio of the significant GO terms. GO analysis confirms the propensity of *neuroLNC* to be in proximity of genes related to chemical transmission, regulation of membrane potential, and synapse development. For an extensive list of GOs, see data S1E. (**D**) Summary of RNA targets found in the RNA interactome. (**E**) Summary of most abundant significantly enriched mRNA interactors. All mRNAs are significantly enriched versus the controls ($P < 0.01$), and >15 counts are represented in plot. For a comprehensive list, see data S1F. Among the most enriched mRNAs, three are also significantly enriched in STRING (Search Tool for the Retrieval of Interacting Genes/Proteins) analysis (gray inset, FDR < 0.01). (**F**) Scatter plot of the MS identification of the protein interactors of *neuroLNC*. TDP-43 is the only highly significant hit ($P < 0.001$). For MS data, refer to data S1H. (**G**) Enrichment of TDP-43 in MS experiments, detailing the negative controls (oligos against LacZ and no probe) and RNA purification performed with *neuroLNC* oligos upon ribonuclease (RNase) treatment. (**H**) Reverse experiment, where upon immunoprecipitating TDP-43, the presence of *neuroLNC* was tested by qRT-PCR, and the enrichment versus the housekeeping mRNA glyceraldehyde phosphate dehydrogenase (GAPDH) was calculated. Ab, antibody; IgG, immunoglobulin G. (**I** and **J**) Quantification of the SV exo-endocytosis experiments upon pBI-driven overexpression of either TDP-43, its antisense RNA (to decrease its levels), *neuroLNC*, a mutated form of *neuroLNC* that does not contain UG-repeats and does not bind TDP-43 (*neuroLNC^MUT*), or several combinations of these constructs. SV exo-endocytosis as in Fig. 1 (B and C), following either a 60- or 600-AP field stimulation at 20 Hz. Down-regulation of TDP-43 blocks the effects of *neuroLNC* at both 60 and 600 AP. The *neuroLNC^MUT* shows no effect on SV exo-endocytosis. In both schemes below, graph significances are summarized. One-way ANOVA followed by Bonferroni's multiple comparison test (*$P < 0.05$; **$P < 0.01$; and ***$P < 0.001$). LFQ, label-free quantification.
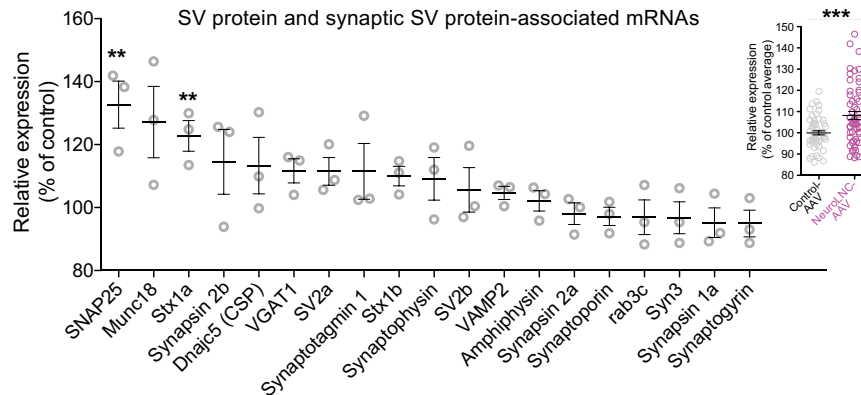
Fig. 6. *NeuroLNC* overexpression increases the levels of SV protein and SV protein–associated mRNAs. Results of the qRT-PCR following overexpression of *neuroLNC* in primary hippocampal neurons with an AAV. Data were GAPDH-normalized and expressed as relative increase with respect to the control cultures (infected with a control AAV). Considering individual mRNA species, only SNAP25 and Stx1a are significantly increased across all tested SV and SV-associated mRNAs. Statistical test, one-way ANOVA followed by Bonferroni's multiple comparison test versus controls (**$P < 0.01$). An overall analysis of the relative expression of all the SV and SV-associated mRNAs against their expression in the controls shows a highly significant increase of the whole class ($8.2 \pm 1.8\%$ increase), suggesting that the effect on all these mRNAs has a limited amplitude but is overall consistent, and single significant differences are probably too small to emerge because of the modest sampling depth. Statistical test, two-tailed Student's *t* test (***$P < 0.001$).

of TDP-43 to take place. Both of these events might result in the specific change of mRNA levels for key proteins in neuronal function. We tested this hypothesis by quantitative real-time PCR (qRT-PCR), where we examined the synaptic mRNAs that were mostly affected by AAV-mediated *neuroLNC* overexpression. When taken singularly, only SNAP25 and Syntaxin-1a were significantly, although modestly, increased (Fig. 6). As a side observation, because of the role of SNAP25 in the control of voltage-gated calcium channels (*30*), at least some of the observed calcium effects might be directly influenced by the differential expression of SNAP25. The class of mRNAs coding for SV proteins and SV protein–associated proteins was, as a whole, significantly increased upon *neuroLNC* overexpression (Fig. 6), while all other classes of synaptic and activity-related mRNAs tested were indistinguishable from the control (fig. S6).

DISCUSSION

The complex developmental programs of neurons rely on finely tuned regulatory mechanisms, which shape the architecture of brain circuits during synapse formation and stabilization. The establishment of neurotransmission, exemplified by SV exo-endocytosis and neurotransmitter release, has a direct influence on these regulatory mechanisms (*31*). Previous studies have revealed that hundreds of lncRNAs are dynamically regulated during neuronal development, brain activity, and synapse plasticity (*5*, *32*, *33*). Nevertheless, these observations often lack a causal relationship, and a direct link between lncRNA expression and SV exo-endocytosis has never been previously elucidated. To study this issue in detail, here we designed a strategy comprising a bioinformatic approach and a subsequent biological assay that quantifies SV release. Our strategy allowed us to identify *neuroLNC*, a nuclear lncRNA that not only regulates SV release but also influences other key aspects of neuronal physiology such as Ca^{2+} dynamics, neurite growth, and neuronal migration.

The initial bioinformatic strategy that we used enabled us to narrow down the most promising candidates that we then studied in detail with more time-consuming techniques on primary neurons. An obvious downside of our approach is that, although we specifically searched for keywords related to neurotransmission and brain plasticity, there is no direct correspondence between the broad terms used in the literature and the phenotypic behaviors of cells. This might explain why at the completion of our screening only one of the candidates turned out to influence the SV recycling assay that we used. Some of the search terms that are used for the bioinformatic screening may encompass different molecular mechanisms. Thus, we cannot exclude that some of the lncRNAs that we initially selected can still influence aspects of neuronal physiology that were not revealed by our biological validation. An obvious improvement for similar bioinformatic strategies would be to sample literature terms directly linked to more technical experimental aspects. At the same time, since we lack highly standardized experimental procedures for the moment, this might not improve the discovery success rate of the approach. Despite these limitations, the dual strategy that we describe here can be adapted to individual experimental needs and has the potential of serving as a blueprint for several future lncRNA studies.

Our screening led to the identification of *neuroLNC*, an activity-dependent lncRNA, which is developmentally regulated and localizes to the nucleus of neurons. One of the criteria that we used for the refinement of the initial bioinformatic results was a certain degree of conservation between humans and rodents, which would suggest that *neuroLNC* function is also conserved across species. An important observation is that, in contrast to several other developmentally regulated lncRNAs, its expression persists throughout adulthood, as observed in rat and human. This indicates that its role might be maintained in adult neurons, where it may contribute to activity regulation and structural plasticity. While this initial work focused on the developmental aspects of *neuroLNC*, future experiments will be necessary to elucidate its role in synapse maintenance and presynaptic plasticity.

Because of the large structural heterogeneity of lncRNAs, their mechanisms of action are extremely diverse (*11*). Natural antisense transcripts (NATs) are one of the most characterized subclasses of lncRNAs since they target protein-coding genes and directly destabilize their respective mRNAs through an antisense mechanism. In the brain,

notable examples include the mRNA of the brain-derived neurotrophic factor (BDNF) and of the potassium voltage-gated channel A2 (KCNA2), which are targeted by two NATs (BDNF-AS and KCNA2-AS) and influence neuronal activity through a direct control of their respective mRNAs (*9*, *34*). We excluded the possibility that *neuroLNC* acts as a NAT by characterizing in detail the genomic region from which it originates.

Our data show that *neuroLNC* is harbored in the vicinity of *miR-124-1*, but it is transcribed from an independent TSS and does not influence the stability or the processing of the neighboring miRNA (Fig. 2). For these reasons, *neuroLNC* should be defined as a large/long intergenic or intervening ncRNA. It is possible to speculate that the regulation of *neuroLNC* itself might take advantage of an antisense mechanism, since we also found some transcripts arising from the opposite direction in the *neuroLNC* locus. This remains for the moment hypothetical, although it is particularly interesting since it might be the basis of the feedback mechanism regulating its level during neuronal hyperactivation (Fig. 3G).

For lncRNAs that do not overlap as an antisense with a protein-coding mRNA in cis, defining the molecular mechanism of action remains extremely challenging (*35*), as also evidenced by the fact that the function of most lncRNAs remains unknown. One of the first steps to define the molecular role of lncRNAs is to identify their molecular interactors (*11*). This task is simplified by the subcellular localization of lncRNAs. *NeuroLNC* is strictly nuclear, and its most likely interactors include DNA, RNA, and proteins. We embarked in three systematic and unbiased screenings to describe the possible interactome of *neuroLNC*. Our screenings reveal that in vivo, the endogenous *neuroLNC* binds the DNA and the RNA of several neuronal genes implicated in neurotransmitter release, synapse organization, glutamatergic signaling, and regulation of neuritogenesis. While this does not narrow down the number of possible mechanisms of action, our findings on the physiology of neurons suggest that *neuroLNC* promotes the transcription of these genes and/or the stabilization of the mRNAs that are bound. We are aware that the validation of all these possible molecular interactions largely exceeds the purpose of this work; thus, we concentrated on the pathways that could explain the effects of *neuroLNC* on neurotransmission. We found that some key mRNAs regulating vesicle release such as SNAP25 and Syntaxin 1 are increased by overexpression (Fig. 6) and are also found interacting with *neuroLNC* (Fig. 5E). This is critical since SNAP25 and Syntaxin 1 are the target SNAREs (soluble *N*-ethylmaleimide–sensitive factor attachment protein receptors) promoting SV fusion.

Very few other lncRNAs have been directly linked to both neuronal excitability and neuronal growth and development. The most notable example is GM12371 (*10*), which shares several similarities with *neuroLNC*, including activity dependency, nuclear localization, and ability to modulate neurite complexity. At the same time, the two lncRNAs seem to have completely different mechanisms of actions, especially because the effects of GM12371 seem to be linked mostly to a postsynaptic phenotype, in contrast with the presynaptic modulation induced by neuroLNC.

An important finding is that *neuroLNC* binds the neurodegeneration-associated protein TDP-43 and that *neuroLNC*^{MUT}, where the UG-repeats were substituted, is unable to potentiate SV release. This indicates that TDP-43 binding is essential for the activity of *neuroLNC*, as is also reinforced by the observation that the down-regulation of TDP-43 abolishes the effects of *neuroLNC* overexpression. Which is the precise molecular pathway that is regulated by the interaction between *neuroLNC* and TDP-43? This question is particularly difficult to address, also in light of the fact that TDP-43 modulates multiple RNA-related processes in the nucleus. These include the regulation of transcription, splicing, and RNA stability, as well as ncRNA processing (*36*). As an example, the activity-dependent lncRNA *Gomafu* might work in a similar manner, since it seems to serve as a scaffold that retains splicing factors that are released upon transient stimulation (*32*). Also in the case of *Gomafu*, the exact mechanism(s) of its function are not yet known. Moreover, TDP-43 participates in liquid-liquid and liquid-solid phase separation processes, influencing the structure of nuclear paraspeckles and of nuclear organization (*37*). *NeuroLNC* may influence any of these processes and possibly function as a scaffold for the assembly of macromolecular complexes that define the specificity of TDP-43 for presynaptic mRNAs, which result in their selective translation and/or stabilization. All these possibilities remain hypothetical and will require future experiments.

Aside from the precise details of the molecular pathway(s) that are regulated by the interaction between *neuroLNC* and TDP-43, one can speculate about the possible clinical significance of *neuroLNC* with respect to diseases such as FTLD and ALS. Future studies in humans should aim at determining whether *neuroLNC* expression is modified in the early stages of these diseases. Moreover, *neuroLNC* may be included in the detailed panel of DNA sequences analyzed in patients with FTLD and ALS. Similarly, it may be worthwhile assessing whether overexpression or down-regulation of *neuroLNC* in animal models modulates the development of TDP-43 proteinopathies and possibly influences the solubility of TDP-43 and/or modifies its interactome. Although promising, clinical applications related to *neuroLNC* should be carefully evaluated and will require future validations.

In conclusion, our results suggest that *neuroLNC* is involved in a feed-forward mechanism that enhances neurotransmission through the regulation of a subset of synaptic RNAs (summarized in fig. S7). More broadly, our work supports the idea that lncRNAs are pertinent for the regulation of neurotransmitter release and that their study may shed new light on the principles that govern neuronal physiology and degeneration.

MATERIALS AND METHODS
Bioinformatic screening
GAMMA is a previously developed algorithm (*14*) to identify correlated transcripts across microarray experiments. After the most correlated transcripts are identified, an entity-based literature-mining approach (*38*) is used to analyze their literature commonalities and predict ncRNA function. We considered the top 40 most highly correlated coding transcripts with the ncRNAs under scrutiny, and we analyzed their literature commonalities. These commonalities include terms such as diseases, chemicals, phenotypes, other genes, cellular functions, cellular structures, and biological processes, similar to GO associations. Thus, when function is not known, these transcriptional correlation networks can be used to infer function, tissue specificity, cellular localization, and phenotype and help prioritize experimentation. The use of GAMMA to successfully predict mRNA function has been previously reported in several other instances, but this is the first successful test of the approach to predict ncRNA functions. GAMMA was used to search for uncharacterized non-coding transcripts associated with the literature annotations: "Brain

development," "Synaptic vesicle," "Synaptic vesicle exocytosis," "Synaptic vesicle endocytosis," "Regulation of synaptic plasticity," "Synaptogenesis," "Neurotransmission," "Dendritic spine," and "Neuronal protein." These terms were used to define a "Guilt by association score" (data S1A) that was used during the first selection round. The filters used for scoring the transcripts were (i) low coding potential (as previously defined) (39); (ii) conservation across species, defined as percentage homology; (iii) distance from the TSS of a known annotated protein-coding gene; and (iv) size (sequences longer than 5 kb were excluded for obvious practical constraints).

Animal and human samples

All animal experiments were approved by the local authority, the Lower Saxony State Office for Consumer Protection and Food Safety (Niedersächsisches Landesamt für Verbraucherschutz und Lebensmittelsicherheit) and the institutional ethical boards of the Katholieke Universiteit Leuven. Mixed neuroglial cultures were prepared from P2 Wistar rats. For *neuroLNC*, cloning and mRNA isolation samples were also collected from Wistar rats at various ages (as indicated in the respective experiments). For in utero electroporation, Swiss mice were used. All human midbrain samples were obtained from the Parkinson's U.K. Brain Bank (Imperial College London, London, England). Snap-frozen tissue blocks were transported and stored under controlled temperature conditions ($-80°C$). The samples were conceded to the Department of Neurology of the University Medical Center Göttingen (Göttingen, Germany), and ethical approval was given by the Multicentre Research Ethics Committee (07/MRE09/72).

Cell culture and transfections

Mixed hippocampal neuroglial cultures and pure glia cultures were prepared from P2 rats as previously described (21). Neurons (between 10 and 14 DIVs) were transfected with the calcium-phosphate ProFection transfection kit (Promega, Fitchburg, WI, USA) as previously described (21). The use of this kit increased the reproducibility over time. Briefly, cells were incubated for 30 min in 37°C fresh Dulbecco's modified Eagle's medium (DMEM complemented with 10 mM $MgCl_2$ and 5 mM Hepes at pH 7.5). For each coverslip, 50 μl of transfection mixture containing 2.5 μg of plasmid DNA, 200 mM $CaCl_2$, and 1× Hepes-buffered solution was applied. The cultured neurons were incubated with the transfection mixture for 20 min at 37°C and 5% CO_2 followed by three washes with fresh DMEM. Coverslips were placed back into their original culture medium and were cultured for 3 days at 37°C and 5% CO_2 to allow transgene expression or down-regulation of the targets before further analyses. Human embryonic kidney (HEK) 293T, C6, and PC-12 cell lines were purchased from the German National Resource Center for Biological Material (DSMZ) and cultured following the recommended conditions. For transfection, PC-12 and C6 cells were detached by trypsin treatment and transfected using the SF cell line 4D-Nucleofector Kit (Lonza) following the instructions of the manufacturer. Following electroporation, transfected cells were seeded and incubated for 3 days at 37°C. The efficiency of down-regulation through TDP-43 antisense (TDP-43-AS) was tested in C6 cells followed by qRT-PCR for TDP-43. Differentiation of PC-12 cells was induced 1 day after transfection with plates coated with collagen (2 μg/ml; Roche) by adding 0.1% horse serum and nerve growth factor RPMI medium (50 ng/ml). To induce differentiation, PC-12 cells were cultured in this medium for 7 days, and the medium was changed every second day. Differentiation was assessed by morphological changes (neurite formation).

Plasmids, shRNAs, and DNA cloning

For all the oligonucleotide primers used during cloning, please refer to data S1J. Note that all plasmids were confirmed by sequencing and, upon reasonable request, they are available from the authors. The bidirectional pBI-CMV1 vector was purchased from Clontech (CA, USA) and modified with the QuikChange II Site-directed mutagenesis kit (Agilent, CA, USA) to delete the Bgl II restriction site within the multiple cloning site no. 1 (MCS1). The VAMP-2 pHluorin sequence was designed in silico on the basis of a previous publication (15), and it was ordered at GenScript (USA) and inserted in the MCS1 upon digestion with Kpn I and Not I. The plasmid encoding for the tetanus toxin light chain (pGEMTEZ-TetTxLC) was a gift from R. Jahn. TetTxLC or the six lncRNAs (data S1B) were inserted in the MCS2 of the pBI-CMV1-pHluorin plasmid with a PCR strategy upon either pGEMTEZ-TetTxLC or Rat genomic DNA amplification. The cloning primers used in the PCR strategy for insertion into the MCS2 added the following couples of restriction sites during amplification: Bcl I/Spe I (for TetTxLC and uc003wst.1), Bgl II/Xba I (uc021rvu.1, uc004bbl.1 and uc003jrq.3), Bgl II/Spe I (uc001pyz.3), or Bam HI/Xba I (uc004bdv.3). The X1 variant of rat TDP-43 (NCBI Reference Sequence: XM_006239382.3) was PCR-amplified from rat complementary DNA (cDNA) to add the Xba I and Sac II restriction sites and was inserted into the pBI-CMV1-pHluorin plasmid construct. For cloning of TDP-43-AS, the PCR fragment was inserted in antisense orientation using Bsu36 I and Sac II restrictions. The plasmid ensured an efficient reduction in TDP-43 expression levels with respect to control-transfected C6 cells as tested by qRT-PCR (fig. S5E). For in utero overexpression, *neuroLNC* was subcloned into the pCAGEN vector (obtained from Addgene) with a PCR strategy adding the Xho I and the Not I restriction sites. For viral overexpression, *neuroLNC* was cloned into an AAV backbone that was previously described (40) allowing the specific expression in neurons (through the human synapsin-1 promoter). For cloning in the viral vector, we used a PCR strategy allowing the addition of the restriction sites Asc I (also known as Sgs I) and Sbf I (also known as Sda I). Positive viral clones were always tested for the integrity of their inverted terminal repeats. For down-regulation, shRNAs against rat and mouse sequences were designed using the Biosettia tool (available at http://biosettia.com/support/shrna-designer/, Biosettia, CA, USA) and cloned following the manufacturer's instructions into the pRNA1-M6-green plasmid [Biosettia; expressing green fluorescent protein (GFP) concomitantly with the shRNA]. As a negative control, the scramble vector provided by Biosettia was used. Note that among several tested down-regulation methods only the use of the mouse U6 pol-III promoter for the expression of shRNAs was efficiently down-regulating *neuroLNC*. The *neuroLNC^MUT* sequence was designed in silico (as specified in data S1I) and was ordered at GenScript (USA). For all subclonings, we relied on commercial chemically competent bacteria (α-select bronze competent cells, Bioline or SURE bacteria from Agilent in case of adeno-associated viral constructs). For transformation, 50 μl of bacteria was heat-shocked at 42°C for 35 s and cooled briefly before addition of 400 μl of Super Optimal broth with Catabolite repression (SOC) medium (Sigma-Aldrich). After incubation for 45 min at 37°C and shaking at 300 rpm, cells were centrifuged and plated on agar plates with the appropriate antibiotic selection. Colonies were picked on the following morning and grown in LB. Midi preps were

prepared using the Macherey-Nagel NucleoBond Xtra Midi EF Kit according to the low copy number protocol. DNA was eluted in double-distilled ultrapure water (ddH$_2$O). Quality and amount of DNA were assessed by NanoDrop 2000 spectrophotometer (Thermo Fisher Scientific).

Virus preparation

Recombinant AAV particles were generated as described before (*41*). Briefly, vectors were propagated in HEK293T cells using the pDP6 helper plasmid (avoiding adenoviral contamination). Viral particles were purified by iodixanol step gradient centrifugation followed by heparin affinity chromatography. Fast protein liquid chromatography–purified/concentrated vectors were desalted by dialysis against phosphate-buffered saline (PBS). Viral titer was adjusted by serial dilution on primary hippocampal neurons by monitoring GFP expression levels (always expressed in a second cassette of the construct, driven by the human synapsin-1 promoter).

SV exo-endocytosis evaluation and calcium imaging

SV exo-endocytosis assays were performed as previously described (*21*, *42*). Neurons were stimulated with an electric field generated in custom-made chambers housing 18-mm coverslips with platinum electrodes (8-mm distance between electrodes). For the generation of the electrical impulses, we used a Stimulus Isolator combined with an A310 Accupulser Stimulator (both from World Precision Instruments, USA) with an initial nominal output of 100 mA. Stimulation was performed either on neurons expressing the bidirectional series of pBI-CMV1-pHluorin plasmids (VAMP-2 based) or coexpressing the orange mOr2-Synaptophysin (mOr2-SypHy) indicator of SV recycling (*21*) together with the Biosettia plasmids for down-regulation. Coexpression was always confirmed by imaging both the enchanced GFP and the mOr2 channel. To test the efficiency of the pBI-CMV1-pHluorin plasmids, we included, in the initial screening, a version encoding the TetTxLC, which cleaves VAMP-2 and blocks neurotransmitter release. Unless otherwise stated, live experiments were performed in Tyrode's solution [124 mM NaCl, 5 mM KCl, 30 mM glucose, 25 mM Hepes, 2 mM CaCl$_2$, and 1 mM MgCl$_2$ (pH 7.4)] supplemented with 10 μM CNQX (Tocris Bioscience, Cambridge, UK) and 50 μM 2-amino-5-phosphonopentanoic acid (D-AP5; Tocris Bioscience, Cambridge, UK) to avoid spontaneous network activation. At the end of each experiment, 50 mM NH$_4$Cl was applied to evaluate total SV content. Live imaging was performed with an inverted Nikon Ti epifluorescence microscope (Nikon, Tokyo, Japan) equipped with a Plan Apochromat 60× 1.4 numerical aperture oil immersion objective, an HBO-100W lamp, an IXON X3897 Andor camera (Northern Ireland, UK), and an Okolab cage incubator system (Okolab, Ottaviano, Italy) to maintain a constant temperature of 37°C. The system was operated through the NIS-Elements AR software (version 4.20; Nikon). ND2 Images were imported using the Bio-Formats (Open Microscopy Environment) plug-in. For quantifications, the difference in fluorescence intensity before and at the peak of the electrical stimulation (Δ*F*) was normalized to the maximum of fluorescence (*F*$_{max}$) measured upon NH$_4$Cl application. For simplicity, all Δ*F*/*F*$_{max}$ values are expressed as a percentage of the signal measured in control cells (either expressing pBI-CMV1-pHluorin or the scramble shRNA vector from Biosettia). Each experiment (*N*) corresponds to a different neuronal preparation. For each neuronal preparation, the Δ*F*/*F*$_{max}$ values were collected and averaged from ~500 synapses from three or more coverslips. Image analysis was performed by identifying the boutons in the exocytotic hotspots with a custom-made National Institutes of Health ImageJ macro based on the "Time Series Analyzer" ImageJ plugin (available at http://rsbweb.nih.gov/ij/plugins/time-series.html). For visualization of calcium dynamics, neurons were loaded in their own medium for 30 min with the acetoxymethyl ester version of Cal-590 (Cal-590-AM; AAT Bioquest), a fluorescein-based Ca^{2+} indicator with single-photon excitation and emission peak wavelengths of 570 and 590 nm, respectively. After a 10-min reequilibration in their culture medium without dye, coverslips were quickly washed in Tyrode's solution. Neurons were imaged and stimulated in the same settings as for the SV exo-endocytosis assay. Image analysis measuring signal intensities was performed using custom ImageJ macros. Briefly, circular regions of interest were placed on transfected cell bodies (identified by the GFP signal), and fluorescence was background-corrected. For each condition more than eight fields from three different preparations were measured. For the analysis of spontaneous activity, cells were imaged in the absence of CNQX and D-AP5, peaks surpassing baseline noise by at least twofold were recorded, and the frequency was determined. For stimulated activity (in the presence of CNQX and D-AP5), Δ*F* was calculated in a 10-s time frame around the stimulation maximum. Δ*F* was then normalized to the baseline signal measured just before the beginning of the stimulation (*F*$_0$). For all experiments with *neuroLNC* overexpression, we also performed the analysis of the fluorescence at the peak maximum (which, depending on the timing of the imaging and of the stimulation, might be slightly shifted in different experiments).

Pharmacology

For the pharmacological modulation of neuronal activity, we used 1 μM TTX (Na$^+$ Channel blocker; Cayman Chemical, USA), 20 μM bicuculline methobromide (GABA$_A$ receptor antagonist; Tocris Bioscience, Cambridge, UK), 100 μM 4-AP (K$^+$ channel blocker; Tocris Bioscience, Cambridge, UK), 10 μM CNQX (AMPA/kainate receptor antagonist; Tocris Bioscience, Cambridge, UK), and 50 μM D-AP5 (*N*-methyl-D-aspartate receptor antagonist; Tocris Bioscience, Cambridge, UK). A total of >200 neurons from three different cultures were blindly analyzed for each condition.

Neurite elongation assay

Primary hippocampal neuron cultures were transfected at 10 DIVs with either a pool of three shRNAs or the pBI construct to down-regulate or overexpress *neuroLNC*, respectively. A total of >20 neurons per condition were analyzed following 4 days of expression, from three independent cultures. Neurons were manually traced in a blind experimental design and analyzed with the ImageJ plugin NeuronJ. The aspects considered were the average length and the number of primary, secondary, and tertiary neurites (arising respectively from the cell body, from a primary neurite, or from a secondary neurite).

In utero electroporation

Pregnant Swiss mice (E14.5) were anaesthetized by intramuscular injections of solution containing 117 μg of ketamine (Anesketin, Eurovet) and 0.7 μg of medetomidine hydrochloride (Domitor, Pfizer) per gram of body weight. Uterine horns were exposed, and a mixture of the required plasmids (1 to 2 μg/μl) was microinjected with the "Fast Green" dye (Sigma-Aldrich) in the lateral ventricles of embryos. Five current pulses (50-ms pulse/950-ms interval) were delivered across the head of the embryos (36 V), targeting the dorsal-medial part of

the cortex. After 3 days of expression, the mothers were euthanized, the embryos were dissected, and the brains were quickly perfused with PBS and 4% paraformaldehyde (PFA). After dissection, the brains were post-fixed for 6 to 10 hours in 4% PFA at 4°C. Vibratome sections (100 m) were collected and prepared for imaging. Analysis of cell migration was performed as previously described (23) by dividing the cortical regions in 10 equal bins and by counting the number of positive neuronal nuclei in each bin. Note that also for neurons showed in Fig. 4 (E versus G), there are differences in the migration of neurons in the controls between experiments, as often observed when different control plasmids are used.

Single-molecule RNA in situ hybridization and immunofluorescence

FISH was performed with minor modifications from the method described in the QuantiGene ViewRNA ISH Cell Assay kit (Affymetrix). Briefly, adherent neuronal cultures were washed in Tyrode's solution before being fixed in 4% PFA (Sigma) in PBS. Samples were further washed in PBS, and the detergent solution was provided by the manufacturer. Specific *neuroLNC* or glyceraldehyde phosphate dehydrogenase (GAPDH) oligonucleotide probes were designed and ordered from Affymetrix, diluted in probe diluent solution, and used for the hybridization. Coverslips were incubated upside down on the probe mix solution in a humidified chamber for 3 hours at 40°C. Alternating with washes in SSC buffer (UltraPure SSC, Thermo Fisher Scientific), incubation with the preamplifier, amplifier, and label mix (1:50 in respective diluent; 30 min at 40°C each) followed. Nuclei were stained with DAPI (4′,6-diamidino-2-phenylindole), and coverslips were embedded on object slides in Mowiol (Calbiochem, Merck).

Quantitative real-time PCR

For RNA isolation from cells or rodent tissues, the miRNeasy Mini Kit (Qiagen) was used. First-strand cDNA was synthesized using SuperScript IV (Life Technologies) according to the manufacturer's protocol. For qRT-PCR analyses, the LightCycler 480 SYBR Green I Master kit (Roche) was used on a LightCycler 480 Instrument II (Roche). All amounts were normalized to their GAPDH controls. miRNA expression level was assessed using the miQPCR method as previously described (19). For human samples, midbrain blocks were transferred shortly to a cryostat for the sake of having controlled temperature conditions during sampling (−20°C). Tissue punches were extracted from the frozen blocks using a 20-G Quincke Spinal Needle (Becton Dickinson), and the sampled material (around 20 mg) was stored into ribonuclease (RNAse)/deoxyribonuclease-free tubes. Total RNA was isolated from the samples using TRI Reagent (Sigma-Aldrich) following the manufacturer's protocol. RNA precipitates were reconstituted in 15 μl of nuclease-free water, and the samples were cleaned and concentrated using the column-based RNA Clean & Concentrator-5 KIT (Zymo Research). RNA (1 μg) from each patient sample was reverse-transcribed using the QuantiTect Reverse Transcription Kit (Qiagen). cDNA samples were diluted 1:3 in nuclease-free water and kept at −20°C until further use. For human GAPDH, we used the primers "Hs_GAPDH_1_SG" provided in the QuantiTect Primer Assay (QT00079247). Unless otherwise stated, all other primers used in this study are summarized in data S1J.

Library preparation and sequencing

Library preparation for mRNA sequencing was performed as previously described (43). Library preparation for ChIRP sequencing was

performed according to the NEBNext Ultra DNA Library Prep Kit for Illumina (New England BioLabs). Libraries were tested for quality and quantified using a NanoDrop 2000 (Thermo Fisher Scientific) and an Agilent 2100 Bioanalyzer (Agilent Technologies). Single-end 50–base pair (bp) sequencing data were generated on an Illumina HiSeq2000 using Illumina TruSeq SBS kits.

RNA-sequencing analysis

Quality assessment was based on the raw reads using the FASTQC (v0.10.1). The sequence reads (single-end 50 bp) were aligned to the rat reference genome (Rnor_6.0) with Bowtie2 (v2.0.2) using RSEM (v1.2.29) with default parameters. First, the rat reference genome was indexed using the Ensembl annotations (v83.6) with rsem-prepare-reference from RSEM software. Next, rsem-calculate-expression was used to align the reads and quantify the gene and isoform abundance. The output of rsem-calculate-expression separately gives the read count and transcripts per million value for each gene and isoform. The enrichment was at the end calculated for each biological experiment separately as summarized in data S1F. Briefly, the enrichment was defined for the odd and the even set separately, and an average enrichment was calculated across all enriched conditions.

ChIRP DNA analysis

Data were analyzed as previously described (44). Briefly, reads were aligned to the rat reference genome (Rnor_6.0) using Bowtie (v2.0.2) with default parameters allowing for two mismatches using seed alignment. Subsequently, aligned reads were filtered for high-quality, uniquely, and multimapped reads (MAPQ ! = [0, 2, 3, 4]). High-quality BAM files were merged for each condition using samtools (v0.1.18). Peak calling was performed using MACS2 (v2.1.2) with a minimum false discovery rate of 0.05. Peaks were assigned to the genes using PAVIS if they were located within 5 kb upstream of the TSS or in the transcribed region or within 1 kb downstream of the transcription end site.

GO and STRING analyses

GO analysis was conducted using WebGestalt using as a reference list all mapped entrez gene IDs from the selected (rnorvegicus) genome. For significance, we used an adjusted P value < 0.05 using the Benjamini-Hochberg method for controlling the false discovery rates during GO terms in biological processes. For details, please refer to data S1E. STRING analysis was conducted as previously described (43). Also in this case, for testing significance, we relied on an adjusted P value < 0.05 using the Benjamini-Hochberg method for controlling the false discovery rates.

5′-RACE PCR

For rapid amplification of 5′-cDNA ends, the GeneRacer Kit with SuperScript III RT and the TOPO TA Cloning Kit for Sequencing (Invitrogen) were used. The gene-specific primers (data S1J) were designed for the 5′ end amplification, and nested PCR products were cloned and sequenced for analyses as reported in data S1C.

ChIRP and RNA interactome analysis

ChIRP and RNA interactome experiments were performed as previously described (24, 26). Antisense oligo probes with 3′ biotin-triethyleneglycol modification (TEG) were designed using the online probe designer on the ChIRP Probe Designer (version 4.2, LGC Biosearch Technologies, Middlesex, UK) and synthesized by Sigma-Aldrich

(data S1J). Note that the designed primers were blasted against whole rat genome and do not specifically bind other targets than *neuroLNC*. The 10 designed probes for *neuroLNC* were divided into two tiling pools (arbitrarily defined odd and even pools). We also designed 10 LacZ probes, which served as negative controls. We performed the *neuroLNC* enrichment from the brain of 2-day-old (P2) rats where neuroLNC expression is high. For ChIRP, cerebral cortices were homogenized with a micropestle in 500 μl of ice-cold low-sucrose buffer [0.32 M sucrose, 5 mM CaCl₂, 5 mM Mg(Ac)₂, 0.1 mM EDTA, 50 mM Hepes (pH 8), 1 mM dithiothreitol (DTT), and 0.1% Triton X-100]. Subsequently, the cortex homogenate was cross-linked with either 3% formaldehyde or 1% glutaraldehyde and sonicated for either 30 or 120 min for either ChIRP MS or ChIRP DNA/RNA, respectively. Enrichment of *neuroLNC* was tested by qRT-PCR for ChIRP RNA samples. ChIRP-derived RNA and DNA were sequenced, and eluted proteins were analyzed by MS proteomics as previously described (*43*).

MS identification of protein interactors following ChIRP/RNA interactome analysis

For proteomic analysis, we initially reversed the cross-linking by boiling the beads in a final concentration of 1× NuPAGE LDS Sample Buffer (Thermo Fisher Scientific) at 95°C for 30 min on a thermomixer (at 750 rpm). After boiling, the samples were loaded on precast NuPAGE 4 to 12% Bis-Tris Protein Gels (Thermo Fisher Scientific) and separated for 20 min at constant voltage (200 V). The gels were stained overnight with Coomassie G250, and for each lane, five to six pieces were cut. In-gel digestion was performed overnight using trypsin. Samples were dried, and peptides were resuspended in 5% acetonitrile and 0.05% trifluoroacetic acid. Samples were further processed for liquid chromatography–MS in an online UltiMate 3000 RSLCnano high-performance liquid chromatography system (Thermo Fisher Scientific) coupled online to an Orbitrap Fusion Tribrid MS instrument (Thermo Fisher Scientific). Peptides were desalted on a reversed-phase C18 precolumn (3 cm long; inner diameter, 100 μm; outer diameter, 360 μm) for 3 min. After 3 min, the precolumn was switched online with the analytical column (~30 cm long; inner diameter, 75 μm) prepared in-house using ReproSil-Pur C18 AQ 1.9-μm reversed-phase resin. The peptides were separated with a linear gradient of 5 to 50% buffer B (80% acetonitrile and 0.1% formic acid) at a flow rate of 10 nl/min over 58-min gradient time. The temperature of the precolumn and the column was set to 50°C during chromatography. The MS data were acquired by scanning the precursors in a mass range from 380 to 1500 Da at a resolution of 120 K at a mass/charge ratio of 200. The acquired RAW data were analyzed using MaxQuant software on the basis of the Andromeda search engine. The updated rat UniProt database was used for identifying proteins (visit the PRIDE dataset identifier PXD013434 for details).

RNA immunoprecipitation

For confirming the interaction between *neuroLNC* and TDP-43, we used a RIP protocol. For this purpose, the cortices of P2 rats were homogenized by a micropestle in low-sucrose buffer [0.32 M sucrose, 5 mM CaCl2, 5 mM Mg(Ac)₂, 0.1 mM EDTA, 50 mM Hepes (pH 8), 1 mM DTT, and 0.1% Triton X-100] on ice. The lysate was cross-linked by 1% formaldehyde and neutralized with 1.25 M glycine. In the following steps, the lysate was washed two times with 1 ml of cold Nelson-Jameson buffer (150 mM NaCl, 20 mM EDTA, 50 mM tris, 0.5% NP-40, and 1% Triton-X-100) and incubated in lysis buffer

[100 mM tris-HCl (pH 8), 20 mM EDTA, and 2% SDS] for 10 min at 4°C. The lysate was precleared with Dynabeads protein A (Invitrogen) and then incubated with rabbit anti-rat TDP-43 antibody (Proteintech, no. 10782-2-AP) or Syntaxin 1A (SYnaptic SYstem, no. 110 302) as a negative control overnight and with beads for additional 1.5 hours at 4°C. After several washing steps, RNA was eluted from beads and purified by an miRNeasy Mini Kit (Qiagen). To achieve high-quality samples, RNAse inhibitor (SUPERase.In, Invitrogen) and protease inhibitors (phenylmethylsulfonyl fluoride and Roche cOmplete EDTA-free protease inhibitor cocktail) were added to all solutions. The purified RNA was either sequenced or reverse-transcribed for qRT-PCR analyses.

Western blot

Beads derived from ChIP were resuspended in 11 μl of Laemmli Buffer (4×) and boiled for 30 min at 95°C before dilution with water. Western blot for TDP-43 protein was performed using the mouse anti-rat TDP-43 (Abcam, no. 104223) and donkey anti-mouse IgG IRDye 800CW (Licor).

Immunocytochemistry

Primary neuron coverslips were washed with Tyrode's solution, fixed with 4% PFA for 40 min, and quenched with glycine (1 M) for 20 min. Afterward, neurons were permeabilized with PBS containing 0.1% Triton and stained with primary and secondary antibodies in PBS containing 1.5% bovine serum albumin and 0.1% Triton for 1 hour. Mouse anti-rat TDP-43 (Abcam, no. 104223) and donkey anti-mouse cyanine3 (Dianova) were used as primary and secondary antibodies, respectively. Imaging was performed using an epifluorescence Nikon Eclipse Ti-E microscope equipped with an HBO-100W Lamp and an IXON X3897 Andor Camera. Capture settings were adjusted with the Nikon Imaging Software (NIS Elements).

Statistical analysis and graph construction

Depending on the data, we used Student's *t* test or analyses of variance (ANOVAs; one or two ways) followed by Bonferroni's multiple comparison post test (as indicated in each figure). Data distribution was assumed to be normal. Equal variances were formally tested and showed no difference between the groups. No statistical methods were used to predetermine sample sizes, and data were collected and processed randomly. Data analysis was performed blind to the condition when possible, and most of the times experiments were independently performed by two or more authors. Box-plot graphs were constructed with the box portion of the plot defined by the 25th and the 75th percentile, and the line dividing the box corresponds to the median. Whiskers indicate the 90th and the 10th percentile.

SUPPLEMENTARY MATERIALS

REFERENCES AND NOTES

1. P. Kapranov, J. Cheng, S. Dike, D. A. Nix, R. Duttagupta, A. T. Willingham, P. F. Stadler, J. Hertel, J. Hackermüller, I. L. Hofacker, I. Bell, E. Cheung, J. Drenkow, E. Dumais, S. Patel, G. Helt, M. Ganesh, S. Ghosh, A. Piccolboni, V. Sementchenko, H. Tammana, T. R. Gingeras, RNA maps reveal new RNA classes and a possible function for pervasive transcription. *Science* **316**, 1484–1488 (2007).

2. K. Struhl, Transcriptional noise and the fidelity of initiation by RNA polymerase II. *Nat. Struct. Mol. Biol.* **14**, 103–105 (2007).

3. Y. Miao, S.-Y. Xu, L.-S. Chen, G.-Y. Liang, Y.-P. Pu, L.-H. Yin, Trends of long noncoding RNA research from 2007 to 2016: A bibliometric analysis. *Oncotarget* **8**, 83114–83127 (2017).

4. A. Sanchez Calle, Y. Kawamura, Y. Yamamoto, F. Takeshita, T. Ochiya, Emerging roles of long non-coding RNA in cancer. *Cancer Sci.* **109**, 2093–2100 (2018).

5. J. A. Briggs, E. J. Wolvetang, J. S. Mattick, J. L. Rinn, G. Barry, Mechanisms of long Non-coding RNAs in mammalian nervous system development, plasticity, disease, and evolution. *Neuron* **88**, 861–877 (2015).

6. G. Barry, J. A. Briggs, D. W. Hwang, S. P. Nayler, P. R. J. Fortuna, N. Jonkhout, F. Dachet, J. L. V. Maag, P. Mestdagh, E. M. Singh, L. Avesson, D. C. Kaczorowski, E. Ozturk, N. C. Jones, I. Vetter, L. Arriola-Martinez, J. Hu, G. R. Franco, V. M. Warn, A. Gong, M. E. Dinger, F. Rigo, L. Lipovich, M. J. Morris, T. J. O'Brien, D. S. Lee, J. A. Loeb, S. Blackshaw, J. S. Mattick, E. J. Wolvetang, The long non-coding RNA NEAT1 is responsive to neuronal activity and is associated with hyperexcitability states. *Sci. Rep.* **7**, 40127 (2017).

7. A. C. Ayupe, A. C. Tahira, L. Camargo, F. C. Beckedorff, S. Verjovski-Almeida, E. M. Reis, Global analysis of biogenesis, stability and sub-cellular localization of lncRNAs mapping to intragenic regions of the human genome. *RNA Biol.* **12**, 877–892 (2015).

8. D. Bernard, K. V. Prasanth, V. Tripathi, S. Colasse, T. Nakamura, Z. Xuan, M. Q. Zhang, F. Sedel, L. Jourdren, F. Coupier, A. Triller, D. L. Spector, A. Bessis, A long nuclear-retained non-coding RNA regulates synaptogenesis by modulating gene expression. *EMBO J.* **29**, 3082–3093 (2010).

9. F. Modarresi, M. A. Faghihi, M. A. Lopez-Toledano, R. P. Fatemi, M. Magistri, S. P. Brothers, M. P. van der Brug, C. Wahlestedt, Inhibition of natural antisense transcripts in vivo results in gene-specific transcriptional upregulation. *Nat. Biotechnol.* **30**, 453–459 (2012).

10. B. L. Raveendra, S. Swarnkar, Y. Avchalumov, X.-A. Liu, E. Grinman, K. Badal, A. Reich, B. D. Pascal, S. V. Puthanveettil, Long noncoding RNA GM12371 acts as a transcriptional regulator of synapse function. *Proc. Natl. Acad. Sci. U.S.A.* **115**, E10197–E10205 (2018).

11. H. Cao, C. Wahlestedt, P. Kapranov, Strategies to annotate and characterize long noncoding RNAs: Advantages and pitfalls. *Trends Genet.* **34**, 704–721 (2018).

12. B. S. Clark, S. Blackshaw, Long non-coding RNA-dependent transcriptional regulation in neuronal development and disease. *Front. Genet.* **5**, 164 (2014).

13. S. Kaech, G. Banker, Culturing hippocampal neurons. *Nat. Protoc.* **1**, 2406–2415 (2006).

14. J. D. Wren, A global meta-analysis of microarray expression data to predict unknown gene functions and estimate the literature-data divide. *Bioinformatics* **25**, 1694–1701 (2009).

15. S. Sankaranarayanan, D. De Angelis, J. E. Rothman, T. A. Ryan, The use of pHluorins for optical measurements of presynaptic activity. *Biophys. J.* **79**, 2199–2208 (2000).

16. P. Johnsson, L. Lipovich, D. Grandér, K. V. Morris, Evolutionary conservation of long non-coding RNAs; sequence, structure, function. *Biochim. Biophys. Acta* **1840**, 1063–1071 (2014).

17. M. Lagos-Quintana, R. Rauhut, A. Yalcin, J. Meyer, W. Lendeckel, T. Tuschl, Identification of tissue-specific microRNAs from mouse. *Curr. Biol.* **12**, 735–739 (2002).

18. T. L. Dill, F. J. Naya, A hearty dose of noncoding RNAs: The imprinted DLK1-DIO3 locus in cardiac development and disease. *J. Cardiovasc. Dev. Dis.* **5**, 37 (2018).

19. V. Benes, P. Collier, C. Kordes, J. Stolte, T. Rausch, M. U. Muckentaler, D. Häussinger, M. Castoldi, Identification of cytokine-induced modulation of microRNA expression and secretion as measured by a novel microRNA specific qPCR assay. *Sci. Rep.* **5**, 11590 (2015).

20. J. L. Knauss, T. Sun, Regulatory mechanisms of long noncoding RNAs in vertebrate central nervous system development and function. *Neuroscience* **235**, 200–214 (2013).

21. S. Truckenbrodt, A. Viplav, S. Jähne, A. Vogts, A. Denker, H. Wildhagen, E. F. Fornasiero, S. O. Rizzoli, Newly produced synaptic vesicle proteins are preferentially used in synaptic transmission. *EMBO J.* **37**, e98044 (2018).

22. S. S. Rosenberg, N. C. Spitzer, Calcium signaling in neuronal development. *Cold Spring Harb. Perspect. Biol.* **3**, a004259 (2011).

23. A. Gärtner, E. F. Fornasiero, S. Munck, K. Vennekens, E. Seuntjens, W. B. Huttner, F. Valtorta, C. G. Dotti, N-cadherin specifies first asymmetry in developing neurons. *EMBO J.* **31**, 1893–1903 (2012).

24. C. Chu, J. Quinn, H. Y. Chang, Chromatin isolation by RNA purification (ChIRP). *J. Vis. Exp.* **61**, 3912 (2012).

25. N. Rani, T. J. Nowakowski, H. Zhou, S. E. Godshalk, V. Lisi, A. R. Kriegstein, K. S. Kosik, A Primate lncRNA mediates notch signaling during neuronal development by sequestering miRNA. *Neuron* **90**, 1174–1188 (2016).

26. C. Chu, Q. C. Zhang, S. T. da Rocha, R. A. Flynn, M. Bharadwaj, J. M. Calabrese, T. Magnuson, E. Heard, H. Y. Chang, Systematic discovery of Xist RNA binding proteins. *Cell* **161**, 404–416 (2015).

27. E. B. Lee, V. M.-Y. Lee, J. Q. Trojanowski, Gains or losses: Molecular mechanisms of TDP43-mediated neurodegeneration. *Nat. Rev. Neurosci.* **13**, 38–50 (2011).

28. A. Bhardwaj, M. P. Myers, E. Buratti, F. E. Baralle, Characterizing TDP-43 interaction with its RNA targets. *Nucleic Acids Res.* **41**, 5062–5074 (2013).

29. K.-J. Tsai, C.-H. Yang, Y.-H. Fang, K.-H. Cho, W.-L. Chien, W.-T. Wang, T.-W. Wu, C.-P. Lin, W.-M. Fu, C.-K. J. Shen, Elevated expression of TDP-43 in the forebrain of mice is sufficient to cause neurological and pathological phenotypes mimicking FTLD-U. *J. Exp. Med.* **207**, 1661–1673 (2010).

30. D. Pozzi, I. Corradini, M. Matteoli, The control of neuronal calcium homeostasis by SNAP-25 and its impact on neurotransmitter release. *Neuroscience*, (2018) [Online ahead of print].

31. L. C. Andreae, J. Burrone, The role of neuronal activity and transmitter release on synapse formation. *Curr. Opin. Neurobiol.* **27**, 47–52 (2014).

32. G. Barry, J. A. Briggs, D. P. Vanichkina, E. M. Poth, N. J. Beveridge, V. S. Ratnu, S. P. Nayler, K. Nones, J. Hu, T. W. Bredy, S. Nakagawa, F. Rigo, R. J. Taft, M. J. Cairns, S. Blackshaw, E. J. Wolvetang, J. S. Mattick, The long non-coding RNA Gomafu is acutely regulated in response to neuronal activation and involved in schizophrenia-associated alternative splicing. *Mol. Psychiatry* **19**, 486–494 (2014).

33. L. Lipovich, F. Dachet, J. Cai, S. Bagla, K. Balan, H. Jia, J. A. Loeb, Activity-dependent human brain coding/noncoding gene regulatory networks. *Genetics* **192**, 1133–1148 (2012).

34. X. Zhao, Z. Tang, H. Zhang, F. E. Atianjoh, J.-Y. Zhao, L. Liang, W. Wang, X. Guan, S.-C. Kao, V. Tiwari, Y.-J. Gao, P. N. Hoffman, H. Cui, M. Li, X. Dong, Y.-X. Tao, A long noncoding RNA contributes to neuropathic pain by silencing Kcna2 in primary afferent neurons. *Nat. Neurosci.* **16**, 1024–1031 (2013).

35. R. E. Andersen, D. A. Lim, Forging our understanding of lncRNAs in the brain. *Cell Tissue Res.* **371**, 55–71 (2018).

36. A. Prasad, V. Bharathi, V. Sivalingam, A. Girdhar, B. K. Patel, Molecular mechanisms of TDP-43 misfolding and pathology in amyotrophic lateral sclerosis. *Front. Mol. Neurosci.* **12**, 25 (2019).

37. S. Maharana, J. Wang, D. K. Papadopoulos, D. Richter, A. Pozniakovsky, I. Poser, M. Bickle, S. Rizk, J. Guillén-Boixet, T. M. Franzmann, A. Jahnel, L. Marrone, Y.-T. Chang, J. Sterneckert, P. Tomancak, A. A. Hyman, S. Alberti, RNA buffers the phase separation behavior of prion-like RNA binding proteins. *Science* **360**, 918–921 (2018).

38. J. D. Wren, R. Bekeredjian, J. A. Stewart, R. V. Shohet, H. R. Garner, Knowledge discovery by automated identification and ranking of implicit relationships. *Bioinformatics* **20**, 389–398 (2004).

39. Y.-J. Kang, D.-C. Yang, L. Kong, M. Hou, Y.-Q. Meng, L. Wei, G. Gao, CPC2: A fast and accurate coding potential calculator based on sequence intrinsic features. *Nucleic Acids Res.* **45**, W12–W16 (2017).

40. L. Sousa-Ferreira, M. Garrido, I. Nascimento-Ferreira, A. Nobrega, A. Santos-Carvalho, A. R. Álvaro, J. Rosmaninho-Salgado, M. Kaster, S. Kügler, L. Pereira de Almeida, C. Cavadas, Moderate long-term modulation of neuropeptide Y in hypothalamic arcuate nucleus induces energy balance alterations in adult rats. *PLOS ONE* **6**, e22333 (2011).

41. J. M. I. Malik, Z. Shevtsova, M. Bähr, S. Kügler, Long-term in vivo inhibition of CNS neurodegeneration by Bcl-X_L gene transfer. *Mol. Ther.* **11**, 373–381 (2005).

42. E. F. Fornasiero, A. Raimondi, F. C. Guarnieri, M. Orlando, R. Fesce, F. Benfenati, F. Valtorta, Synapsins contribute to the dynamic spatial organization of synaptic vesicles in an activity-dependent manner. *J. Neurosci.* **32**, 12214–12227 (2012).

43. E. F. Fornasiero, S. Mandad, H. Wildhagen, M. Alevra, B. Rammner, S. Keihani, F. Opazo, I. Urban, T. Ischebeck, M. S. Sakib, M. K. Fard, K. Kirli, T. P. Centeno, R. O. Vidal, R.-U. Rahman, E. Benito, A. Fischer, S. Dennerlein, P. Rehling, I. Feussner, S. Bonn, M. Simons, H. Urlaub, S. O. Rizzoli, Precisely measured protein lifetimes in the mouse brain reveal differences across tissues and subcellular fractions. *Nat. Commun.* **9**, 4230 (2018).

44. R. Halder, M. Hennion, R. O. Vidal, O. Shomroni, R.-U. Rahman, A. Rajput, T. P. Centeno, F. van Bebber, V. Capece, J. C. G. Vizcaino, A.-L. Schuetz, S. Burkhardt, E. Benito, M. N. Sala, S. B. Javan, C. Haass, B. Schmid, A. Fischer, S. Bonn, DNA methylation changes in plasticity genes accompany the formation and maintenance of memory. *Nat. Neurosci.* **19**, 102–110 (2016).

Citation: S. Keihani, V. Kluever, S. Mandad, V. Bansal, R. Rahman, E. Fritsch, L. C. Gomes, A. Gärtner, S. Kügler, H. Urlaub, J. D. Wren, S. Bonn, S. O. Rizzoli, E. F. Fornasiero, The long noncoding RNA *neuroLNC* regulates presynaptic activity by interacting with the neurodegeneration-associated protein TDP-43. *Sci. Adv.* **5**, eaay2670 (2019).

Science Advances

The long noncoding RNA *neuroLNC* regulates presynaptic activity by interacting with the neurodegeneration-associated protein TDP-43

S. Keihani, V. Kluever, S. Mandad, V. Bansal, R. Rahman, E. Fritsch, L. Caldi Gomes, A. Grtner, S. Kgler, H. Urlaub, J. D. Wren, S. Bonn, S. O. Rizzoli, and E. F. Fornasiero

View the article online
https://www.science.org/doi/10.1126/sciadv.aay2670
Permissions
https://www.science.org/help/reprints-and-permissions

Use of this article is subject to the Terms of service